International Journal for Housing Science and Its Applications
Publish August 4, 2025. Volume 46, Issue 3 Pages 3410-3427

https://doi.org/10.70517/ijhsa463288

Simulation analysis of external characteristics of medium voltage flexible interconnection system and research on protection strategy based on multi-intelligent body system

Shijin Xin[1,*], Kan Feng[2], Guojie Hao[3], Xiaofeng Wang[4], Qing Xu[3] and Libao Wei[3]
[1] Energy Development Research Center, Baiyin Power Supply Company, Baiyin, Gansu, 730900, China
[2] Party Committee, Baiyin Power Supply Company, Baiyin, Gansu, 730900, China
[3] Development Planning Department, Baiyin Power Supply Company, Baiyin, Gansu, 730900, China
[4] Dispatching Center, Baiyin Power Supply Company, Baiyin, Gansu, 730900, China
Corresponding authors: (e-mail: w18032636560@yeah.net).

Abstract The flexible interconnection of the distribution network based on flexible DC and the hybrid AC-DC distribution network structure will bring great changes and challenges to the traditional operation mode of the distribution system. Based on combing the structure of MV DC distribution system and flexible interconnection device, the article proposes the control model of converter station of flexible interconnection system based on MMC and constructs the operation strategy of flexible interconnection system. The stability of the MV flexible interconnection system is simulated and analyzed by combining the output impedance model and equivalent circuit of the DC side of the flexible converter. In order to further improve the control effect of the MV flexible interconnection system accessing the distribution network, this paper combines the multi-intelligent body (MMC) system with the flexible interconnection control strategy, constructs the control and protection strategy of the MV flexible interconnection system accessing the distribution network, and carries out the simulation analysis of it. The results show that obvious resonance peaks can be observed in the Bode diagram of MMC, and the simulated measured and theoretical curves are in good conformity, and the optimized balanced control strategy of capacitor voltage of MMC sub-module can realize the balanced control of capacitor voltage and the amplitude of voltage fluctuation can be controlled within ±5% of the rated voltage of the capacitor. Relying on the system control and protection strategy established in this paper, the energy management control effect of the distribution network can be significantly ensured and the reliability of the distribution network can be enhanced.

Index Terms medium voltage DC distribution system, flexible interconnection device, MMC, output impedance model, multi-intelligent body system, control and protection strategy

I. Introduction

With China's “dual-carbon” goal, the extensive access to new types of sources and loads represented by photovoltaic and electric vehicles has become an important feature of the development and construction of China's urban energy Internet. On the one hand, the distributed power with intermittency and randomness has transformed the traditional distribution network from “limited power” to “ubiquitous power”, changing the distribution of grid current and system operation characteristics, and the two-way current regulation and control of the distribution network is facing new challenges [1]-[3]. On the other hand, large-scale DC charging loads with impact and disorder put great pressure on the capacity of distribution grids, resulting in an imbalance between the supply and demand of local electric power [4]-[6]. These factors have challenged the safe and stable operation of distribution grids, and there is an urgent need for advanced distribution technologies to support them, and to improve the adaptability and compatibility of distributed power sources while meeting diversified power needs [7], [8].

In recent years, with the rapid development of power electronics technology and the mature application of high-voltage DC transmission, DC technology has begun to extend to the medium and low voltage fields. Medium-voltage DC (MVDC) distribution has begun to receive attention because of its advantages of high power supply quality, flexible trend control, and adaptation to AC and DC friendly access, and has gradually become a popular topic for research and demonstration applications as the cost of power electronic equipment continues to decline [9], [10]. The interconnection of conventional MV AC distribution networks based on MVDC distribution technology can realize asynchronous combined loop operation between AC distribution feeders without increasing the short-circuit capacity, achieve load balancing and flexible transfer of tidal current, and improve the power supply reliability of the MV distribution network and its ability to consume distributed energy and energy storage [11]-[14]. However, MVDC

flexible interconnected distribution system lacks rotating equipment inside, and the system inertia is small, which is easy to cause various types of oscillations or even induce instability, resulting in significant economic losses [15]-[17]. Therefore, it is necessary to analyze and study the stability of MVDC flexible interconnected distribution system by constructing a multi-intelligent body system [18].

Flexible interconnection technology can reconfigure the distribution network topology, realize the closed-loop connection between different feeders, and enhance the stable and economic operation of the distribution network. In this paper, based on the typical structure of DC distribution network, the control model of key equipment and the operation strategy of flexible interconnection system are established by combining the flexible interconnection device and modular multilevel converter (MMC). The small-signal method is used to establish the mathematical model of DC output impedance for MMC, and the stability of the system is simulated by MATLAB software with the equivalent circuit of the MV flexible interconnection system. In addition, based on the flexible interconnection control strategy, this paper introduces the multi-intelligent body system to establish the control and protection strategy of the MV flexible interconnection system, and verifies its control effect and access reliability.

II. Medium voltage DC distribution system and impedance modeling

In the traditional "passive" distribution network, the regulation and control methods (such as transformer on-load voltage regulation, capacitor switching) are relatively limited, and it is difficult to solve the new problems arising in the complex "active" distribution network. On the other hand, with the rapid development of power electronics technology, communication control technology, and energy storage technology, making full use of these technologies to carry out "active" management of the "active" distribution network can effectively improve the operation of the distribution network system and promote the consumption of renewable energy. Based on the flexible and flexible interconnection topology, it can realize the autonomous coordination and control of distributed energy units such as intermittent new energy and energy storage devices, actively absorb renewable energy and ensure the safe and economic operation of the network, improve the utilization rate of distribution network assets, and delay the upgrade investment of the distribution network.

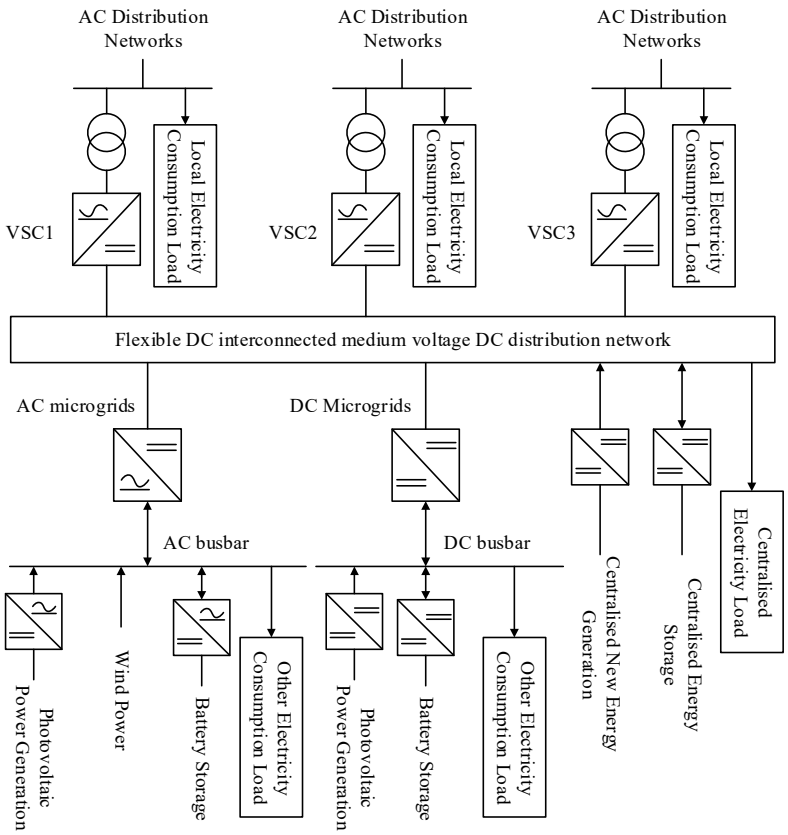

Figure 1: Typical structure of DC distribution system

II. A.Medium Voltage DC Distribution System Structure

II. A. 1) Typical structure of a DC distribution network

The existing or planned DC distribution system demonstration projects are mostly multi-terminal power supply mode. Relevant literature summarizes seven typical application scenarios of DC distribution system from high, medium and low voltage levels, among which medium and high voltage DC distribution network can be mainly applied to flexible interconnection of AC distribution network, multi-terminal flexible DC distribution network, and access to large-scale renewable energy power generation and so on. Figure 1 shows the typical medium-voltage DC distribution system structure applicable to the above main application scenarios [19]. In order not to lose the generality, this paper considers the DC distribution network as a three-terminal structure, which is connected to the local AC distribution network through voltage source type converters VSC1~VSC3 and corresponding isolation transformers. The multi-terminal power supply structure can improve the operational reliability of the MV DC distribution network, and more importantly, the structure can realize the flexible interconnection and power flexible control among multiple feeders of the AC distribution network.

Inside the DC distribution network, the following two parts can be connected through DC lines and multi-nodes/busbars:

(1) Centralized AC/DC loads, new energy generation and energy storage systems. The DC distribution network can supply power to centralized AC/DC loads through DC-AC or DC-DC converters, and large-capacity new energy generation systems can also be connected to the DC distribution network through corresponding converters. In order to suppress the power fluctuation of DC distribution network and improve system stability, a certain capacity of energy storage unit can also be configured at the key nodes.

(2) AC/DC microgrid. The user side can integrate local loads, distributed power supply and energy storage system in the form of microgrid, and then connect to DC distribution grid through bidirectional converter, and DC distribution grid and AC/DC microgrid can support each other under emergency conditions.

II. A. 2) Flexible interconnected distribution system structure

At present, research scholars according to different operational scenarios, the network structure of flexible interconnection distribution system is divided into three kinds, the interconnection structure based on back-to-back flexible interconnection device, point-to-point flexible interconnection structure containing DC bus, and AC/DC hybrid interconnection structure based on flexible interconnection device [20].

Flexible interconnection device is the core of flexible interconnection technology, with the continuous updating and iteration of technology, interconnection equipment currently has the following four basic topologies. That is, phase changing converter (LCC) based on half-controlled device thyristor, voltage source converter (VSC) based on fully controlled switchable device IGBT, mid-point clamped (NPC) based on fully controlled IGBT and uncontrollable diode, and modularized multilevel converter (MMC), whose number of levels is determined by the number of sub-modules (SM) put into operation in each phase of the bridge arm.

With the maturity of the flexible DC transmission technology, the flexible technology has been extended to the distribution level as well, thus meeting the demand for high quality power in today's society. In addition, the application of flexible technology for accessing the grid towards distributed power sources, electric vehicle charging piles, etc. has also achieved good results. Thus, the transfer of flexible technology from transmission level to distribution level has rich engineering significance to enhance the reliability of power supply in distribution networks, improve the ability of stable operation of the system, enhance the ability of the grid to absorb distributed power sources, and realize high-quality power supply.

II. B.Modeling of converter station control for critical equipment

II. B. 1) Modular Multilevel Converter

Reasonable design of control system is the key to realize the function of flexible interconnection device. The operation control strategy of flexible interconnection device based on MMC should meet the following requirements:

One is to ensure the stability of DC side voltage, which is the basic premise for the smooth operation of the device and depends on the mutual coordination of the control modes of MMC at each end.

The second is to give full consideration to the operational requirements of the MMC itself, control the voltage and current of various components within the MMC, and take control measures such as loop current suppression, sub-module capacitor voltage equalization control, and capacitor voltage ripple suppression.

In the single-phase equivalent circuit diagram of the MMC, u_{pj} and $u_{nj}\left(j=a,b,c\right)$ denote the upper and lower bridge arm voltages, i_{pj} and i_{nj} represent the upper and lower bridge arm currents, respectively; u_j and i_j represent the AC-side phase voltage and phase current, while U_{dc} and i_{dc} represent the DC-side voltage and

current. The L_0 and R_0 represent the inductance and equivalent resistance of the bridge arm. The neutral point of the AC and DC sides is denoted by "N" and "O" respectively, and the fundamental frequency component of the voltage between the two is 0 under the condition of symmetry of the AC system [21].

According to Kirchhoff's voltage/current law, the mathematical model expression for the MMC is obtained as:

$$\begin{cases} \dfrac{U_{dc}}{2} = u_{pj} + L_0 \dfrac{di_{pj}}{dt} + R_0 i_{pj} + u_j \\ \dfrac{U_{dc}}{2} = u_{nj} + L_0 \dfrac{di_{nj}}{dt} + R_0 i_{nj} - u_j \end{cases} \tag{1}$$

$$i_j = i_{pj} - i_{nj} \tag{2}$$

Define the differential mode component of the upper and lower bridge arm voltages as u_{dif_j} and the common-mode component as u_{com_j}, with the expression:

$$\begin{cases} u_{dif\_j} = \dfrac{1}{2}(u_{nj} - u_{pj}) \\ u_{com\_j} = \dfrac{1}{2}(u_{nj} + u_{pj}) \end{cases} \tag{3}$$

This can be introduced by adding or subtracting the two equations in equation (1):

$$\frac{L_0}{2}\frac{dj_j}{dt} + \frac{R_0}{2} i_j = u_{dif\_j} - u_j \tag{4}$$

$$L_0 \frac{di_{com\_j}}{dt} + R_0 i_{com\_j} = \frac{U_{dc}}{2} - u_{com\_j} \tag{5}$$

where i_{com_j} denotes the common-mode current with the expression:

$$i_{com\_j} = \frac{1}{2}(i_{pj} + i_{nj}) = i_{dc\_j} + i_{cir\_j} \tag{6}$$

where i_{dc_j} denotes the DC component of the common mode current, which can be considered as $i_{\mathrm{dc}}/3$ in the conventional working condition; and i_{cir_j} denotes the internal loop current.

From Eqs. (4) and (5), it can be seen that when the AC-side voltage, DC-side voltage and bridge arm parameters are determined, the MMC output current is mainly controlled by the upper and lower bridge arm differential mode voltages, while the loop current is mainly determined by the upper and lower bridge arm common mode voltages.

The expressions for the upper and lower bridge arm reference voltages $u_{\mathrm{pj,ref}}$ and $u_{\mathrm{nj,ref}}$ are:

$$\begin{cases} u_{pj,ref} = \dfrac{U_{dc}}{2} - u_{dif\_j} - u_{cir\_j} \\ u_{nj,ref} = \dfrac{U_{dc}}{2} + u_{dif\_j} - u_{cir\_j} \end{cases} \tag{7}$$

where u_{cir_j} denotes the additional value of the bridge arm voltage generated by the loop current control.

II. B. 2) Converter Station Control Modeling for MMC

In order to realize the effective control of the MV flexible interconnected distribution system, this paper establishes the converter station control model of the MV flexible interconnected distribution system based on MMC, and its specific equivalent circuit is shown in Fig. 2.

In the figure, L_{T} is the leakage inductance of the converter transformer, $2L$ is the inductance value of the bridge arm, and both of them are determined, $2R$ is the equivalent resistance of the bridge arm, which cannot be determined accurately, u_a, u_b, u_c, and i_a, i_b, and i_c are the voltages and currents on the net side of the converter transformer, respectively, u_{a1}, u_{b1}, u_{c1} and i_{a1}, i_{b1}, i_{c1} are the voltages and currents of the upper bridge arm, respectively. u_{a2}, u_{b2}, u_{c2} and i_{a2}, i_{b2}, i_{c2} are the voltages and currents of the lower bridge arm, and U_{d} and I_{d} are the voltages and currents on the dc side, respectively, each bridge arm contains $SM_1 \sim SM_n$ of n sub-modules, and P, N and O are the positive, negative and neutral points of the DC side, respectively [22].

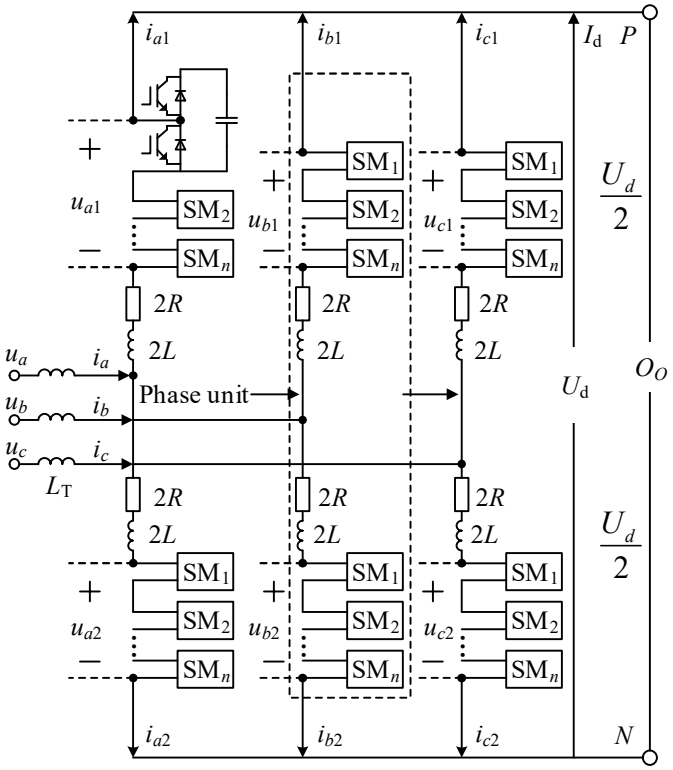

Figure 2: Circuit diagram of MMC converter station

The converter has six bridge arms, each of which consists of n identical submodules and one converter reactance in series, each of which contains two insulated gate bipolar transistors (IGBTs) and a current-continuing diode bank and one energy-storage capacitor. When the upper IGBT of the submodule is turned on and the lower IGBT is turned off, the submodule capacitor is connected to the bridge arm and the submodule is said to be engaged. When the lower IGBT of the submodule is turned on and the upper IGBT is turned off, the submodule capacitance is removed from the bridge arm, and the submodule output voltage is 0, and the submodule is said to be removed. The upper and lower bridge arms of each phase form 1 phase unit, and the DC voltage on the DC side is maintained by the parallel connection of 3 phase units in three phases. In order to ensure that the total DC voltage is stable, the number of submodules in each phase unit in the input state is maintained at n. The desired AC phase voltage output is obtained by changing the distribution relationship of these n submodules between the upper and lower bridge arms of the phase.

This is obtained from Kirchhoff's current law:

$$i_{k1} + i_{k2} = i_k; \quad k = a,b,c \tag{8}$$

The current flowing in the same direction from bottom to top in the upper and lower bridge arms of the k -phase cell can be expressed as

$$i_{kdif} = \frac{i_{k1} - i_{k2}}{2} \tag{9}$$

Let I_{kdc} and i_{kac} be the DC and AC components of i_{kdif} respectively. Then the k -phase upper and lower bridge arm currents can be expressed as respectively:

$$i_{k1} = \frac{i_k}{2} + I_{kdc} + i_{kac} \tag{10}$$

$$i_{k2} = \frac{i_k}{2} - I_{kdc} - i_{kac} \tag{11}$$

Kirchhoff's voltage law is obtained by applying it to the k -phase upper and lower bridge arms, respectively:

$$u_k - \left(\frac{U_d}{2} - u_{k1}\right) = 2L\frac{di_{k1}}{dt} + 2Ri_{k1} + L_T\frac{di_k}{dt} \tag{12}$$

$$u_k - \left(-\frac{U_d}{2} + u_{k2} \right) = 2L\frac{di_{k2}}{dt} + 2Ri_{k2} + L_T\frac{di_k}{dt} \tag{13}$$

This can be obtained by adding Eq. (12) and Eq. (13) and dividing by 2:

$$u_k - \frac{u_{k2} - u_{k1}}{2} = (L_T + L)\frac{di_k}{dt} + Ri_k \tag{14}$$

Let $v_k = (u_{k2} - u_{k1})/2$ and $L_S = L_T + L$.

Then Eq. (14) can be rewritten in the form of a three-phase system, viz:

$$L_S(di_{abc}/dt) = -Ri_{abc} + u_{abc} - v_{abc} \tag{15}$$

where $i_{abc} = [i_a \quad i_b \quad i_c]^T$, $u_{abc} = [u_a \quad u_b \quad u_c]^T$, $v_{abc} = [v_a \quad v_b \quad v_c]^T$.

Equation (15) describes the dynamic characteristics of the AC side of the converter station. Subtracting Eq. (12) from Eq. (13) yields:

$$(u_{k1} + u_{k2}) - U_d - 4RI_{kdc} = 4L\frac{di_{kac}}{dt} + 4Ri_{kac} \tag{16}$$

According to Kirchhoff's current law the DC side current is obtained as:

$$I_d = \sum_{k=a,b,c} (I_{kdc} + i_{kac}) \tag{17}$$

Eqs. (16) and (17) describe the dynamic characteristics of the DC side of the converter station. It can be seen that the AC loop current component i_{kac} is due to the capacitive voltage fluctuation of the series sub-module set, which basically does not contribute to the power delivery.

The above dynamic mathematical model of the MMC converter station is obtained based on Kirchhoff's law, which can be used for controller design, where the dynamic characteristics of the AC side of the MMC converter station are similar to those of a conventional converter. The model is applicable not only to normal state but also to grid fault state, and the effect of leakage reactance of the converter transformer is considered.

II. B. 3) Flexible Interconnection System Operation Strategy

According to the state of the AC distribution network and the operating state of the balancing unit within each microgrid subsystem, the MV DC distribution center has a variety of operating modes, and the basic premise of its operation control is to ensure the stability of the MV DC bus voltage, the LV DC microgrid bus voltage, the LV AC microgrid bus voltage and frequency, as well as to realize the switching of the operating modes of the various subsystems in the case of faults.

(1) Mode I: Normal operation mode

In the normal operation mode, the internal units of the three subsystems are in normal operation. The MV DC distribution center bus voltage is controlled by the MMC, and the DC microgrid bus voltage, AC microgrid bus voltage, and AC frequency are controlled by the energy storage units within the respective systems. the MMC and DC transformer receive power scheduling commands, and work in the power scheduling mode in order to coordinate and control the interconnection power between the AC microgrid, DC microgrid, and MV DC distribution center.

(2) Mode II: AC/DC microgrid mode supported by MV/DC distribution center

In this operation mode, the AC distribution grid and MMC are in normal state, which can ensure the normal voltage of ±10kV DC bus. In this case, if the DC microgrid subsystem is normal and the energy storage unit of the AC microgrid subsystem is faulty, then the DC transformer works in the interconnection power control mode and the MMC works in the AC microgrid subsystem support mode to stabilize the AC microgrid bus voltage and frequency. If the AC microgrid subsystem is normal and the energy storage unit in the DC microgrid subsystem is faulty, the MMC operates in the interconnected power control mode, and the DC transformer operates in the DC microgrid subsystem support mode to maintain the DC microgrid bus voltage stabilization. If both the AC and DC microgrid sub-system energy storage units fail, the MMC and DC transformer shall work in the AC microgrid sub-system support mode and DC microgrid sub-system support mode, respectively, to maintain the stability of the AC and DC sub-systems.

(3) Mode III: Medium voltage DC distribution center anomaly mode

In this mode, the AC feeder or MMC is in a fault state, i.e., the MV DC distribution center subsystem can no longer be controlled normally and stably by the three MMCs. In this mode, if both the AC and DC microgrid subsystems are normal, the MMCs and DC transformers can be shut down for operation, i.e., the AC microgrid subsystem and DC microgrid subsystem are working in independent operation mode. If the AC microgrid subsystem or the DC microgrid subsystem energy storage unit fails, the AC and DC microgrid subsystems can work in the mutual support mode.

III. Stability analysis of medium-voltage flexible interconnection systems

Compared with the traditional thyristor-based HVDC transmission system, flexible DC transmission operation is more flexible, the system can be controlled better, and can be sent to the weak AC system or even passive system, which is very suitable for weak system or island power supply, renewable energy and other distributed power generation grid, asynchronous AC grid interconnection, and urban grid power supply and other fields. In the future, with the progress and development of power electronics technology, flexible DC transmission will show its unique advantages in solving the problems faced by long-distance, high-capacity power transmission, new energy distributed power supply access, as well as large-scale AC and DC hybrid power grids. As a new generation of DC transmission technology, flexible DC transmission provides an effective solution for the change of power grid transmission mode and the construction of future power grid.

III. A. Impedance Model and Equivalent Circuit for Medium Voltage Flexible Interconnect System

III. A. 1) Output impedance model of DC side of flexible converter

The flexible converter is composed of several MMCs, and the mathematical model of DC side output impedance is established for MMCs by using the small signal method, and the voltage and current relational equation in the dq-axis coordinate system can be expressed as follows:

$$\begin{cases} L_1 \dfrac{di_d}{dt} = u_d - d_d u_{mmci} + \omega L_1 i_q \\ L_1 \dfrac{di_q}{dt} = u_q - d_q u_{mmci} - \omega L_1 i_d \end{cases} \tag{18}$$

$$C_1 \frac{du_{mmci}}{dt} = \frac{3}{2}(d_d i_d + d_d i_q + d_q i_d + d_q i_q) \tag{19}$$

When a small disturbance occurs in the system, a small signal linearization of Eqs. (18) and (19) is obtained:

$$\begin{cases} L_1 \dfrac{d\hat{i}_d}{dt} = \hat{u}_d - \hat{d}_d U_{mmci} - D_d \hat{u}_{mmci} + \omega L_1 \hat{i}_q \\ L_1 \dfrac{d\hat{i}_q}{dt} = \hat{u}_q - \hat{d}_q U_{mmci} - D_q \hat{u}_{mmci} - \omega L_1 \hat{i}_d \end{cases} \tag{20}$$

$$C_1 \frac{d\hat{u}_{mmci}}{dt} = \frac{3}{2}\left(D_d \hat{i}_d + \hat{d}_d I_d + D_q \hat{i}_q + \hat{d}_q I_q\right) - \hat{i}_o \tag{21}$$

where the letter above with ^ indicates the amount of small signal perturbation of the corresponding physical quantity, the same below, D_d, D_q are the steady-state values of duty cycle at the DC steady-state operating point of d-axis, q-axis, respectively. I_d, I_q are the steady-state values of current at the DC steady-state operating point of d-axis and q-axis, respectively, U_{vsci} is the DC-side steady-state voltage of the i-th MMC, and $\hat{i}_o$ is the injected small-signal perturbation current source.

When the system operates at unit power factor, $u_q = 0$ and $i_q = 0$, and from Eqs. (18) and (19), the I_d, D_d, and D_q of the MMC at the steady state operating point are:

$$I_d = \frac{2P_i}{3U_d} \tag{22}$$

$$D_d = \frac{U_d}{U_{mmci}} \tag{23}$$

$$D_q = -\frac{2\omega L_1 P_i}{3U_d U_{mmci}} \tag{24}$$

where P_i is the transmitted power of the i th MMC.

The small-signal model in the s-domain after the Rasch transform of Eqs. (20) and (21) is:

$$\begin{cases} sL_1 \hat{i}_d = \hat{u}_d - \hat{d}_d U_{mmci} - D_d \hat{u}_{mmci} + \omega L_1 \hat{i}_q \\ sL_1 \hat{i}_q = \hat{u}_q - \hat{d}_q U_{mmci} - D_q \hat{u}_{mmci} - \omega L_1 \hat{i}_d \end{cases} \tag{25}$$

$$sC_1 \hat{u}_{mmci} = \frac{3}{2}(D_d \hat{i}_d + \hat{d}_d I_d + D_q \hat{i}_q + \hat{d}_q I_q) - \hat{i}_o \tag{26}$$

The small-signal impedance model of the MMC is not only related to the topology but also to its control strategy. According to the control strategy in Fig. 2, the small-signal expression for voltage-current control can be obtained as:

$$(\hat{u}_{mmci}^{ref} - \hat{u}_{mmci})G_{uu} = \hat{i}_d^{ref} \tag{27}$$

$$\begin{cases} -(\hat{i}_d^{ref} - \hat{i}_d)G_{iu} + \omega L_1 \hat{i}_q + \hat{u}_d = \hat{d}_d U_{mmci} \\ -(\hat{i}_q^{ref} - \hat{i}_q)G_{iu} - \omega L_1 \hat{i}_d + \hat{u}_q = \hat{d}_q U_{mmci} \end{cases} \tag{28}$$

where $G_{uu} = k_{uup} + k_{uui}/s$, $G_{iu} = k_{iup} + k_{iui}/s$, k_{uup}, k_{uui} are the P parameter and I parameter of the outer loop of the MMC voltage, k_{iup}, k_{iui} are the P parameter and I parameter of the inner loop of the MMC current, respectively.

Combining Eq. (25)-Eq. (28), the MMC AC-side small-signal model, DC-side small-signal model and control system small-signal model can be obtained. Accordingly, the output impedance of the DC side of the MMC can be obtained as:

$$\begin{aligned} Z_{mmcc} = \frac{\hat{u}_{mmci}}{\hat{i}_o} = &\left((sL_1 + G_{iu})U_{mmci}\right) / \left(sC_1 U_{mmci}(sL_1 + G_{iu})\right. \\ &+1.5D_d U_{mmci}(D_d + G_{uu}G_{iu}) - 1.5I_d G_{uu} G_{in}(sL_1 + G_{iu}) \\ &\left.+1.5I_d G_{in}(D_d + G_{uu}G_{iu})\right) \end{aligned} \tag{29}$$

Since the flex converter controls the DC side voltage of the MMC, it is defined as a source converter. Since the parameter settings are the same for each MMC, the output impedance of the MVC port of the flex converter is:

$$Z_{A\_out} = N' Z_{mmci} \tag{30}$$

III. A. 2) Equivalent Circuit for Medium Voltage Flexible Interconnect System

In order to analyze the stability of the flexible interconnected distribution system based on MMC, after obtaining the impedance model, it is necessary to represent the equivalent circuit of this interactive system with a linear network structure, and then the impedance stability criterion is used to analyze the system stability. Fig. 3 shows the small-signal equivalent circuit of the flexible interconnected distribution system based on MMC.

In the figure, $I_g(s)$ is the line current, and U_{eq1_out} and I_{eq2_in} are the equivalent voltage source at the MVDC output side and the equivalent current source at the MVDC input side port, respectively.

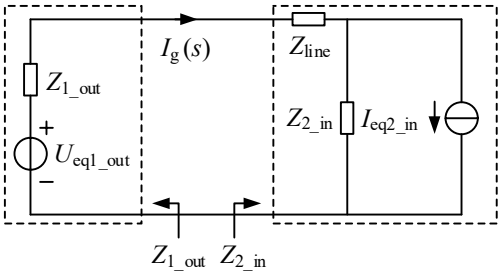

Figure 3: Equivalent circuit of flexible interconnected power distribution system

In analyzing the stability of the cascade system, $I_g(s)$ can be expressed as:

$$I_g(s) = \left(I_{eq2\_in} + \frac{U_{eq1\_out}}{Z_{2\_in}}\right) / \left(1 + \frac{Z_{1\_out}}{Z_{2\_in} + Z_{line}}\right) \tag{31}$$

where the stability of $I_g(s)$ depends on $1/\left[1 + Z_{1\_out}/(Z_{2\_in} + Z_{line})\right]$ when both the source converter and the load converter can be operated stably. Therefore, only $Z_{1\_out}/(Z_{2\_in} + Z_{line})$ satisfies the Nyquist criterion to ensure the stability of MVDC flexible interconnected distribution system. Define the impedance ratio T_m as:

$$T_m = Z_{1\_out} / Z'_{2\_in} \tag{32}$$

Eq. $Z'_{2\_in} = Z_{2\_in} + Z_{line}$.

III. B. Stability Simulation Analysis of Medium Voltage Flexible Interconnect System

III. B. 1) Flexible Interconnection DC Side Impedance Verification

In order to verify the validity of the DC side impedance model of the MV flexible interconnection system established in this paper, this paper builds a nonlinear time-domain simulation system in MATLAB/Simulink simulation platform according to the relevant parameters of the MV flexible interconnection system, and carries out the validation of the DC side impedance model on the basis of the system's ability to operate stably.

The basic method of impedance measurement is to inject a small perturbation signal into a stable operating system, and there are two methods: voltage perturbation and current perturbation. In this paper, the current perturbation injection method is used to calculate the small-signal impedance model using the port perturbation current and the response perturbation voltage, and the measurement principle is shown in Fig. 4. In the figure, i_s is the injected perturbation current source, the source converter and the load converter are connected in parallel with respect to the perturbation current source, $\hat{i}_s$ is the current flowing into the source side, and $\hat{i}_l$ is the current flowing into the load side. Data processing is performed on the dc-side voltage and dc-side current to extract the amplitude information and phase information of the perturbation current and the responsive perturbation voltage at each frequency point. The ratio of the perturbation voltage and the perturbation current flowing into the source converter side is the source converter output impedance Z_{s_out}, and the ratio of the perturbation voltage and the perturbation current flowing into the load converter side is the load converter input impedance Z_{l_in}.

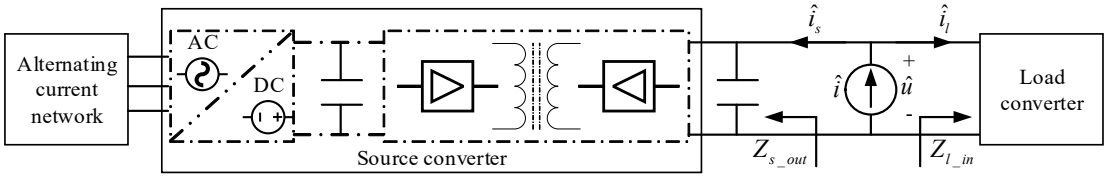

Figure 4: The basic methods of impedance measurement

Fig. 5 shows the Bode plot of DC side impedance. Where Fig. 5(a)~(b) shows the amplitude-frequency and phase-frequency characteristic curves, respectively. Observing the amplitude-frequency characteristic curve and phase-frequency characteristic curve, compared with the traditional VSC, the Bode plot of the MMC can observe the obvious resonance peaks, and the single-stage unity-controlled MMC is more determined by the MMC in the low-frequency band of the output impedance, and more determined by the LLC resonant converter in the high-frequency band of the output impedance. And the simulated real measurements are in good agreement with the theoretical curves, which proves the correctness of the modeling method of flexible interconnected DC distribution system based on MMC proposed in this paper.

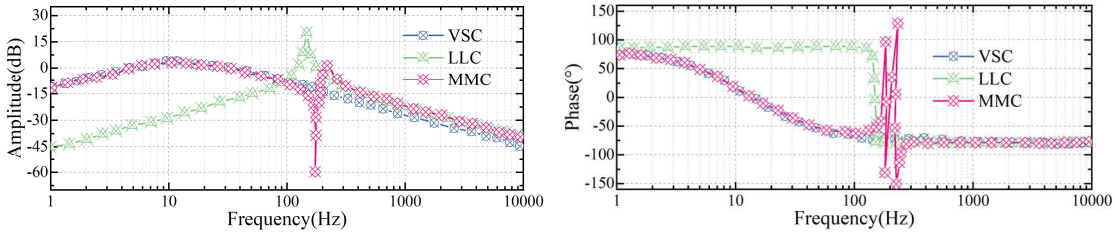

(a) Amplitude-frequency characteristic curve (b) Phase-frequency characteristic curve

Figure 5: The Bode diagram of the DC side impedance

In addition, this paper also simulates the relevant factors affecting the DC side impedance of the flexible interconnect system. There are many factors affecting the DC side impedance, including circuit parameters and controller parameters, such as the DC side voltage regulator capacitance, voltage regulator capacitance of the MMV and LLC connection port, AC side filtering inductance, voltage loop proportionality coefficient, integration coefficient, current loop proportionality coefficient, and integration coefficient. The DC side voltage regulator capacitance has a small effect on the phase frequency characteristic curve, but has a larger effect on the high frequency band of the amplitude frequency characteristic curve, and the impedance amplitude of the high frequency band decreases with the increase of the DC side voltage regulator capacitance, and the MMV and LLC connecting port voltage regulator

capacitance affects the resonance peak before the impedance of the capacitive band, and the impedance amplitude of the band decreases with the increase of the value of the impedance capacitance on the resonance peak before the resonance peak, and the impedance amplitude of the band decreases with the increase of its value. The influence of AC side inductance on the amplitude-frequency characteristic curve and phase-frequency characteristic curve is relatively small, so the influence of AC side inductance on DC side impedance is almost negligible. The voltage loop scale factor mainly affects the DC side impedance Bode plot amplitude-frequency characteristic curve amplitude at the peak size, if the amplitude at the peak is too large, it may be overlapped with the input impedance of the back-end load converter, so that the system generates the risk of oscillation.

III. B. 2) Steady-state control simulation of flexible interconnected systems

In this paper, the control model of MV flexible interconnection converter station based on MMC is proposed and its specific operation strategy is given. Based on the MMC converter station control model constructed in Section 2.2.2, a simple 4-terminal MMC-LLC simulation system is constructed in the PSCAD/EMTDC simulation software, which contains a total of four different converter stations (A, B, C, and D). After the simulation system enters into steady state operation, the reference values of the controller input signals in converter stations B and D are adjusted to verify the effectiveness of the active controllers at the converter station level. The specific experiments are as follows:

(1) When the simulation time is 8s, the reference value of active power in converter station B is adjusted from -80 MW to 80 MW.

(2) When the simulation time is 10s, the reactive power reference value of converter station D is adjusted from -30MVA to 30MVA.

(3) Adjust the AC voltage reference value of converter station B from 230kV to 220kV at simulation time of 12s.

(4) Adjust the load to verify the effectiveness of the passive controller at the converter station level. At simulation time 8s, 2MW of active power as well as 16MVA of reactive power are added and removed at 9.5s to simulate a reactive power impact process.

The simulation results are shown in Fig. 6, where the simulated waveforms of experiments (1) to (4) are shown in Fig. 6(a) to (d).

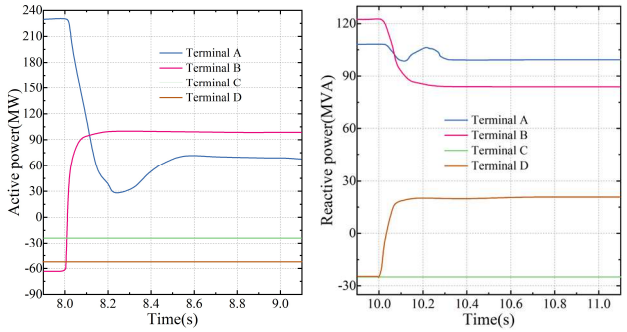

(a) Experiment (1) (b) Experiment (2)

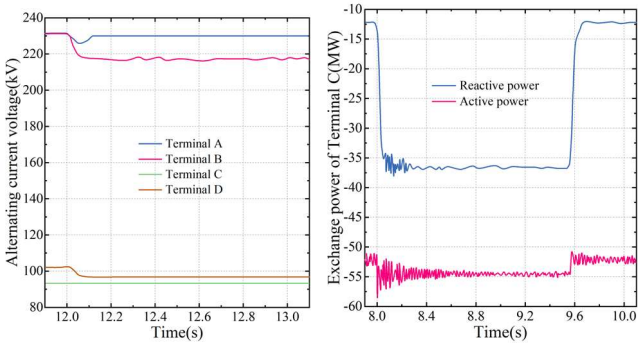

(c) Experiment (3) (d) Experiment (4)

Figure 6: Simulation diagram of system steady-state control

From Fig. 6(a), after the reference value of active power is adjusted at converter station B, the active power of converter station B changes from -80MW to 80MW within 0.2s, and converter station A plays the role of power balancing, and its active power is reduced from 230MW to about 68MW. From Fig. 6(b), after the reference value of reactive power is adjusted at converter station D, the reactive power of converter station D changes from -30MVA to 30MVA within 0.2s, and since there is an electrical connection between converter station A, converter station B, and the AC grid connected to converter station D and converter station A and converter station B adopt the constant AC voltage control method, the reactive power deficit in this part is supplied by converter stations A and B to supplement. From Fig. 6(c), the AC voltage at converter station B is adjusted from 230 kV to 220 kV within 0.2 s after converter station B adjusts the AC voltage reference value. Since converter station B is electrically connected to the AC grid to which converter station D is connected, and since converter station D uses a control method of constant reactive power control, which does not control the voltage of the connected AC grid, the AC voltage at converter station D also drops. From Fig. 6(d), a reactive shock load is introduced at converter station C at 8 s. The passive islanding controller is able to continue to supply power to the islanding stably after the grid load jump. After the shock load is removed, the system can quickly restore stable operation. From the above simulation results, it can be obtained that during the steady state operation of the system, the control system designed in this paper can realize the functions of trend control, AC voltage stabilization, and islanding power delivery of the MMC-LLC system, and the controller has a fast response speed and less fluctuation during the response process.

III. B. 3) Balancing control effects of flexible interconnected systems

Each bridge arm of the MMC converter consists of 10 sub-modules, and the sub-module capacitance voltage is rated at 15kV (there is no fully controlled semiconductor device with such a high voltage level in the project, and the value is taken in the simulation to simulate the larger transmission power in the project under a lower number of levels), and the carrier frequency is set to 300Hz, and the bridge arm reactance of the converter is 34mH, and the sub-module capacitance is set to 3mF. The rated DC bus voltage is ±220kV (the DC bus voltage difference is 440kV), and the rated DC power is set to 540MW. The rated DC bus voltage is ±220kV (the DC bus voltage difference is 440kV), and the rated DC power is set to 540MW. The rectifier side adopts constant DC voltage and constant reactive power control, and the inverter side adopts constant active power and constant reactive power control. The simulation results of the rectifier side are illustrated as an example.

With constant DC side voltage, the voltage waveforms of the upper and lower bridge arms of the MMC-LCC system are verified when the flexible interconnected system operation strategy is adopted, as well as the balancing control effect of the circulating current suppression coefficient and the capacitance equalization coefficient on the capacitance voltage of the submodules in the MMC bridge arms. The simulation results are shown in 7, where Figs. 7(a)~(c) show the balanced control effects of the upper and lower bridge arm voltages, DC voltage, and total harmonic distortion rate, respectively.

From Fig. 7(a), it can be seen that when the MMC adopts the flexible interconnection system operation strategy designed in this paper, the upper and lower bridge arms can be equated as controllable voltage sources, and since the AC side of the MMC is a constant level output at this time, its bridge arm outputs a step waveform with a 21 level. Combined with Fig. 7(b), it can be seen that the optimized balancing control strategy for the capacitor voltage of the MMC sub-module proposed in this paper can realize the balanced control of the capacitor voltage, and the amplitude of the voltage fluctuation is controlled within ±5% of the rated capacitor voltage. Due to the inversion of the modulating waveforms of the upper and lower bridge arms, the sub-module voltage fluctuations can be partially canceled out, and the DC bus voltage fluctuations are small. Fig. 7(c) shows that when the number of MMC levels is higher, the value of the total harmonic distortion rate of its AC-side output phase voltage is smaller. Meanwhile, the smaller average value of the absolute value of the MMC three-phase unit circulating current also indicates that the capacitor voltage optimization and balancing control strategy proposed in this paper can better suppress the MMC phase-to-phase circulating current.

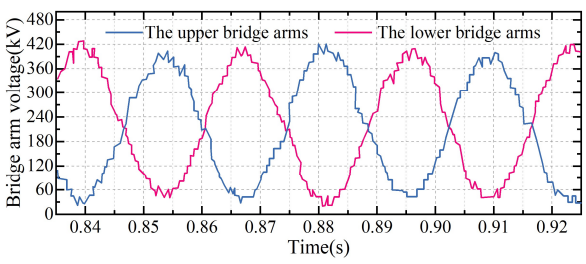

(a) Upper and lower bridge arm voltage

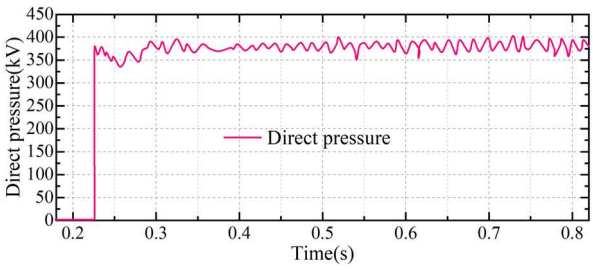

(b) Direct pressure

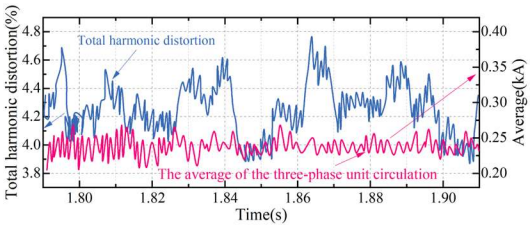

(c) Total harmonic distortion rate

Figure 7: Balance control effect of flexible interconnection systems

IV. Medium-voltage flexible interconnection system control and protection strategies

Medium-voltage flexible DC distribution system can efficiently accept and utilize new energy sources such as photovoltaic, wind power, and DC power sources such as energy storage, and provide efficient and reliable power supply for DC loads such as electric vehicles, data centers, and LED lighting, so it has received wide attention. However, due to the different characteristics of power electronic equipment in the system, complex DC network topology, various control strategies, and frequent changes in the operating state with a wide range of changes, the DC distribution network suffers from multi-timescale small and large disturbance stability problems. Based on this, this chapter proposes a control and protection strategy for the MV flexible interconnection system based on a multi-intelligent body system, which aims to enhance the control and protection of relevant parameters in the distribution network and improve its load regulation capability.

IV. A. Control schemes supported by multi-intelligence systems

IV. A. 1) Multi-intelligent system technology

The control structure of a traditional multi-intelligent body system includes three levels of intelligences, and the first level of connections refers to distributed intelligences such as relay intelligences, distributed generation intelligences, load intelligences, and circuit breaker intelligences. The second level of intelligences includes relay intelligences, distributed generation intelligences, load intelligences, and circuit breaker intelligences. The third level serves as the central processing unit, which is mainly responsible for collecting all transient data related to the network through the second level intelligences, detecting events in the network through the collected data, and sharing the network information among all levels of intelligences based on the detected state data [23].

In a protection scheme based on a multi-intelligent body system, all levels of intelligences can perform the expected functions, collect and exchange data, and execute commands issued by the central processing unit. For example, when a fault occurs at a location in the power network, the relay intelligences first send network data to the central processing unit. The central processing unit then summarizes and analyzes the data from different sources and subsequently sends commands to the relay intelligences to clear the fault and maintain a suitable time margin between the primary and backup relays as quickly as possible[24]-[26].

In a multi-intelligent body system architecture, the IEC-61850 protocol is used to receive and send communication signals and to establish a direct connection between two devices capable of exchanging data within 5ms. In addition, another important protocol in the IEC-61850 standard is the Sampled Measured Value Protocol, which can be used to transmit voltage and current data to help the multi-intelligent body system to share the parameters of the grid in microseconds. Grouping at the intermediate layer using the three levels of control described above is a solution to maintain coordinated operation between devices in the event of a fault, but when the network size is large and the number of intelligentsia increases, the number of states for power system stability will increase significantly. Specifically, it is necessary to define all possible states associated with each intelligence as a pending pattern in order for the system to make decisions and exchange the correct information with each target intelligence.

IV. A. 2) Flexible interconnection control strategies

In the MMC-based flexible interconnected distribution system, when the AC system on both sides connected to the flexible switch is in three-phase symmetrical stability and its power loss is neglected, the power output equation of the flexible switch is:

$$\begin{cases} P_{FTS} = \dfrac{3}{2}(E_d i_d + E_q i_q) - U_{dc} i_{dc} \\ Q_{FTS} = \dfrac{3}{2}(E_q i_d - E_d i_q) \end{cases} \tag{33}$$

When the AC system is in the three-phase balanced steady state, $E_{d1,2}$ is constant, and $E_{q1,2}$ is approximated to be 0. Then, from Eq. (33), it can be seen that the output power of the flexible switching is linearly related to the dq -axis current component. Accordingly, the control system is designed as an internal and external double closed-loop control structure, as shown in Fig. 8.

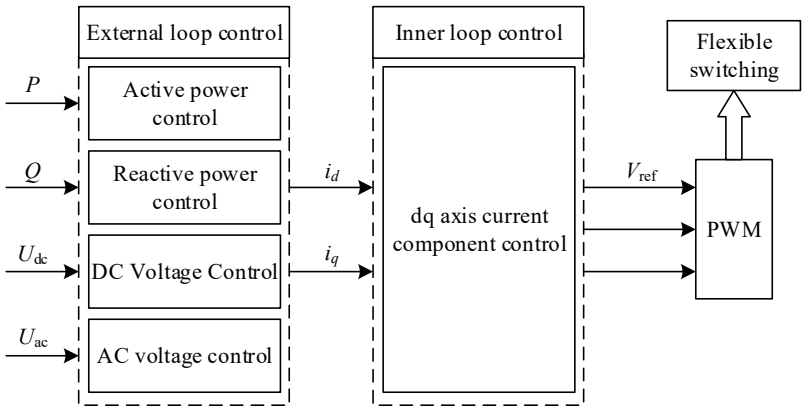

Figure 8: The double closed-loop control strategy of flexible switches

Among them, each outer ring determines the reference value of i_d and i_q components of the grid-side current of the flexible switch according to the upper control target, and the inner ring is used to control the output modulation voltage of the MMC, through the accurate control of the fundamental waveform components of the modulation voltage, the actual output current of the flexible switch can quickly track the reference value of the outer ring, so as to realize the corresponding control target.

The flexible switch can exchange the outer-loop control targets of the MMCs on both sides according to the actual needs to realize the accurate control of the active and reactive power or the terminal voltage on the AC side. However, the active power flowing through the flexible switch can be smoothly transmitted only when the DC side voltage is basically kept constant. Therefore, the control of both sides of the flexible switch needs to be coordinated with each other, usually by one side of the converter to maintain the DC voltage stable, and the other side to regulate the size of the transmitted active power.

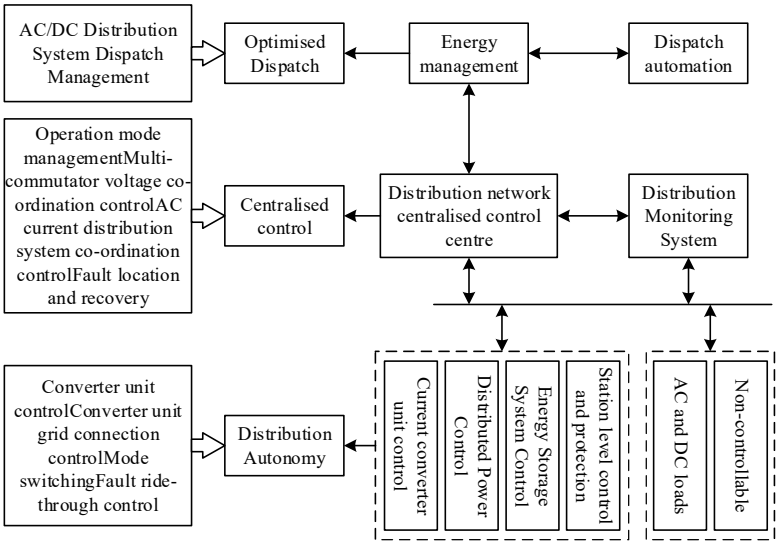

Figure 9: Control and protection system framework

IV. A. 3) System control and protection strategies

The basic function of DC distribution control system is to maintain the power supply reliability and power quality demand of important loads in AC and DC distribution system, and realize the full utilization of distributed power on

this basis. According to the power and voltage control requirements of DC distribution system, combined with the multi-intelligent body system and flexible interconnection control strategy, this paper establishes the framework of multi-terminal medium-voltage flexible interconnection DC distribution control and protection system, and its specific architecture is shown in Figure 9. The DC distribution control and protection system adopts a layered distributed structure with three layers and two networks. The three layers include the optimization scheduling layer, the centralized control layer and the distribution control layer, and the two networks refer to the monitoring and control communication network and the control LAN network used to transmit information among the three layers.

(1) The optimized dispatching layer consists of the operator monitoring system, the operator centralized control system and the dispatching system, through which the monitoring and control of all equipment within the distribution system is completed.

(2) The centralized control layer consists of the energy management system and the DC control master, both of which are based on the multi-intelligent body system. The energy management control host optimizes the load output of each node in the system according to the operation of DC distribution system, and forms the power and voltage control instructions for each control node of DC distribution system. The DC distribution network control master completes the management and switching of the basic operation mode of the distribution system, maintains the power supply reliability and power quality demand of the important loads in the AC and DC distribution system, carries out unified control of the equipment constituting the backbone network frame of the DC distribution system such as the voltage source converter, DC transformer and DC switch, as well as controllable power supply equipments such as the storage battery, etc, and establishes and maintains a stable DC system voltage.

(3) The distribution control layer is the bottom layer control, which consists of control and protection sub-stations, converter node unit control equipment, converter valve equipment and field I/O equipment. Due to the many types of DC distribution system equipment and the large difference in external characteristics, it is necessary to configure different control strategies for different types of equipment.

IV. B. Medium Voltage Flexible Interconnection System Control and Protection Simulation

IV. B. 1) Simulation analysis of system control effect

In order to verify the feasibility of the MV flexible interconnection control and protection strategy based on the multi-intelligent body system proposed in this paper, a simulation model is constructed by using MATLAB/Simulink simulation software, and a multi-terminal flexible interconnection AC/DC distribution system based on multi-terminal flexible interconnection device is constructed with reference to the structure shown in Fig. 1, in which flexible interconnection device contains three flexible interconnection modules, and it is assumed that FIM-A is the main control flexible interconnection module, FIM-B and FIM-C are auxiliary converter modules. FIM-A is assumed to be the main control flexible interconnection module, and FIM-B and FIM-C are auxiliary converter modules. The rated DC bus voltage of the system is 800V, and the voltage variation between the intervals is 15V, the rated AC grid voltage is 400V, the frequency is 60Hz, and the rated load of the system is 80kW.

At the same time, for the above mentioned multi-terminal flexible interconnected AC and DC distribution system of an application example - the future regional energy control center, set different AC power grids with different tariffs, at the same time, the same grid is also divided into peak time, valley time, the usual three different tariffs, the AC grid tariffs as shown in Table 1, which set The electricity price of each AC grid is shown in Table 1, in which the purchasing price and selling price are set to be consistent.

Table 1: Electricity prices of each AC power grid

Power conversion unit	Electricity prices (yuan)		
	Peak time	Usually time	Valley time
FIM-A	1.52	0.94	0.36
FIM-B	1.63	0.83	0.43
FIM-C	1.28	0.72	0.55
PV	0.00	0.00	0.00
ESS	0.00	0.00	0.00

Mode I in the operation strategy of the flexible interconnection system is selected for simulation, which is used to verify the correctness of the system's energy management for the MV DC distribution network. The unit dispatch period of energy management is set to be 10 min, and the total simulation market is 4 h. The simulation time t is set to be valley time tariff in 0~1.1 h, usual time tariff in 1.1~3.1 h, and peak time tariff in 3.1~4 h, and the weighting coefficients of each time period are 0.35, 0.35, and 0.3, respectively. The simulation results are shown in Fig. 10,

and Figs. 10(a)~(h) are respectively DC bus voltage, transmission power of FIM-A, FIM-B and FIM-C, PV transmission power, BES transmission power, load power and battery SOC changes.

When t=0, the system tariff is the valley time tariff, at this moment the grid tariff is relatively high grid output is more, the transmission power of each power conversion unit FIM-A, FIM-B, FIM-C, PV and ESS is 18kW, 22kW, 3.2kW, 6kW and -10kW respectively, the dc bus voltage is maintained by the master flexible interconnection module, the and stabilized at about 774V. Since the battery SOC deviates too much from the normal value, it is in a state of constant charging and its charging power decreases as the SOC situation improves.

When t=1.1h, the system tariff becomes the usual tariff, and more power is transmitted from the grid with relatively high tariff, and each power conversion unit rapidly completes the output adjustment, and the DC bus voltage stabilizes at about 774V after a short fluctuation. At this time, due to the system tariff increase, the cost of energy storage charging increases, and its charging power decreases.

When t=2h, the load power increases to 45.2kW, and according to the layer 3 integrated optimization control instruction, the battery storage unit is converted from charging to discharging, and the output power is about 6.1kW, and at this time, the battery SOC is 55%, but the battery SOC continues to deviate from the optimal value due to the discharging, and therefore, the discharging power of the battery storage unit is gradually decreasing in the subsequent stages.

When t=3h, the light intensity increases to 360kW/m2 and the PV output power increases to 16kW. As the photovoltaic power generation unit out to ease the load pressure, the battery storage system is converted from discharging to charging at this time.

When t=4h, the system tariff becomes peak tariff, the battery storage system converts from charging to discharging in order to reduce the cost of user tariffs, at this time, the battery SOC gradually shrinks to about 48%, and due to the discharging causes the battery SOC to continue to deviate from the optimal value, so the discharging power of the battery storage unit in the subsequent stages gradually decreases.

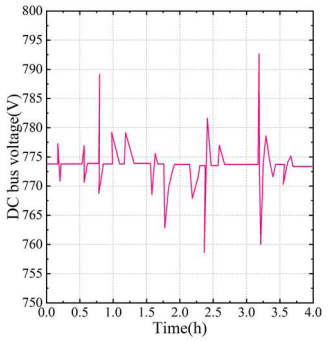

(a) DC bus voltage

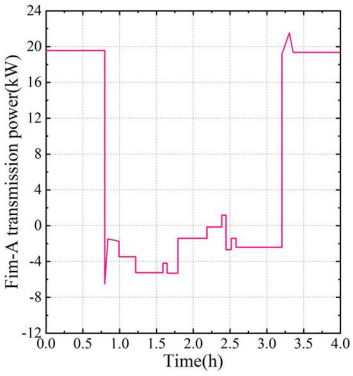

(b) Fim-A transmission power

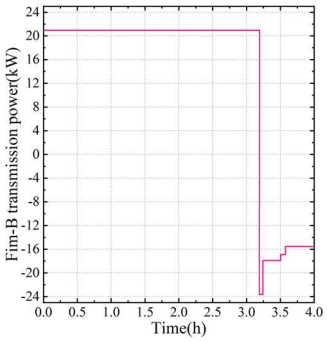

(c) Fim-B transmission power

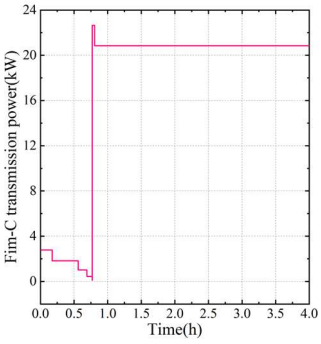

(d) Fim-B transmission power

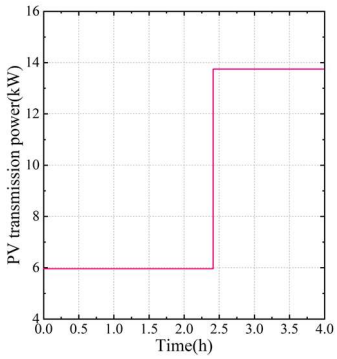

(e) PV transmission power

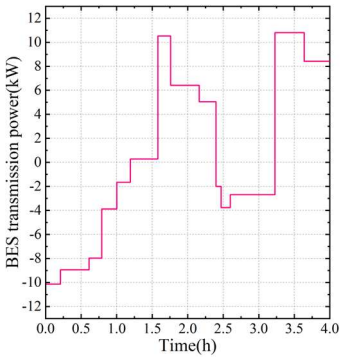

(f) BES transmission power

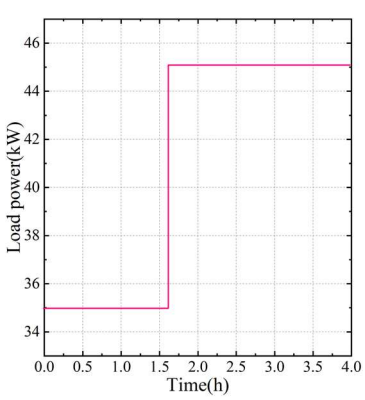

(g) Load power

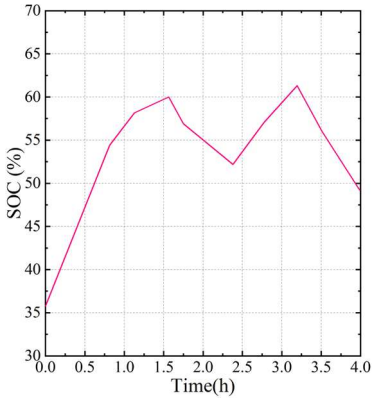

(h) Battery SOC

Figure 10: System operation characteristics in mode Ⅰ

IV. B. 2) Impact of access location on distribution reliability

For the MV flexible interconnected system, its access location in the active distribution network may have an impact on the reliability of the distribution network. Based on this, this paper chooses the rapid reliability assessment method of flexible interconnected distribution network decoupled with sequential sampling and fault analysis to calculate the reliability assessment of the access location of different flexible Internet systems, and its reliability assessment results are shown in Table 2. In the table, SAIFI, SAIDI and ASAI denote the system average outage frequency expectation, system average outage time expectation, and average power supply reliability expectation, respectively.

Table 2: Reliability assessment result

Access mode	SAIFI	SAIDI	ASAI
Access Mode 1	1.537	2.694	0.9992
Access Mode 2	1.908	3.571	0.9986
Access Mode 3	1.269	2.135	0.9995
Not connected	2.046	4.223	0.9981

Network feeder system can significantly improve the system reliability, access mode 3 (all connected to the end of the feeder) has the greatest improvement in system reliability, comparing access mode 3 and FIM without access to the distribution network, after the FIM device access to the distribution network, the system average outage frequency expectation, system average outage time expectation, and the average power supply reliability rate expectation, respectively improved by about 37.98%, 49.44%, and 0.14%. In terms of load level, the access of MV flexible interconnection system devices can significantly improve the reliability level of each load point. Similarly, access mode 3 (all connected at the end of the feeder) has the greatest improvement in the reliability of each load point, and the reliability of its power supply is improved to a certain extent compared with that of the FIM not connected to the distribution network.

Therefore, through the above comparative analysis of the reliability level of the whole system and each load, it can be concluded that the MV flexible interconnection system device can significantly improve the reliability level of the distribution system after it is connected to the active distribution network.

V. Conclusion

The article proposes a flexible interconnection system device based on MMC and models its converter station control strategy to construct the operation strategy of the flexible interconnection system. In order to further ensure the stability and reliability of the active distribution network, this paper proposes a MV flexible interconnection system control and protection strategy combined with a multi-intelligent body system on the basis of the flexible interconnection control strategy. And the control effect and reliability of the MV flexible interconnection system are analyzed by simulation software. From the simulation results, obvious resonance peaks can be observed in the Bode diagram of MMC, and the simulation measured and theoretical curves are in good conformity. During the steady state operation of the system, the trend control of the MMC-LLC system can be realized with the control system designed in this paper, and the controller response speed is fast and the fluctuation during the response process is small. After the FIM device is connected to the distribution network, the expected value of the average outage frequency of the system, the expected value of the average outage time of the system, the expected value of the average reliability rate of the power supply are improved by about 37.98%, 49.44%, and 0.14%, respectively.

The effective combination of the MV flexible interconnection system device and the active distribution network can significantly enhance the stability of the distribution network and further improve the ability to consume distributed energy resources and the application of energy storage technology. The MV flexible interconnection system can be turned into an islanding operation mode, utilizing the power supplied by the lines on the non-faulty side to provide voltage support for the faulty area, minimizing the scope of power outages and improving the overall power supply reliability of the distribution network.

Funding

This project is funded by the Gansu Electric Power Company Science and Technology Project of State Grid in 2024: Research on key Technology and typical configuration of flexible interconnection of Medium voltage Distribution Network (No.: B72703241203).

References

[1] Huang, X., Fang, S., Niu, T., Chen, G., Liao, R., & Wang, Z. (2024). Coordinated Voltage Regulation Strategy for an Energy Storage Integrated Distribution Network in Bidirectional Power Flow Mode. IEEE Transactions on Industry Applications.

[2] Tang, C. Y., Chen, P. T., & Jheng, J. H. (2021). Bidirectional power flow control and hybrid charging strategies for three-phase PV power and energy storage systems. IEEE Transactions on Power Electronics, 36(11), 12710-12720.

[3] Liao, J., Zhou, N., Qin, Z., Wang, Q., & Bauer, P. (2022). Power disequilibrium suppression in bipolar DC distribution grids by using a series-parallel power flow controller. IEEE Transactions on Power Delivery, 38(1), 117-132.

[4] Fu, Q., Du, W., Wang, H., & Xiao, X. (2021). Stability analysis of DC distribution system considering stochastic state of electric vehicle charging stations. IEEE Transactions on Power Systems, 37(3), 1893-1903.

[5] Makrygiorgou, D. I., & Alexandridis, A. T. (2017). Stability analysis of dc distribution systems with droop-based charge sharing on energy storage devices. Energies, 10(4), 433.

[6] Mohamad, A. M., & Mohamed, Y. A. R. I. (2018). Investigation and enhancement of stability in grid-connected active DC distribution systems with high penetration level of dynamic loads. IEEE Transactions on Power Electronics, 34(9), 9170-9190.

[7] Zhao, Y., Jin, Q., Chen, R., Li, H., Yan, J., & Zhang, X. (2024, September). Combined-Loop Operation Control Strategy for Medium-Voltage Distribution Networks Based on Phase Shifter Interconnection. In 2024 China International Conference on Electricity Distribution (CICED) (pp. 603-609). IEEE.

[8] Zhang, X., Cheng, L., Gao, L., Zhang, Y., Li, Z., Zeng, Y., ... & Jiang, X. (2016). Closed-Loop distribution network by a midvoltage flexible HTS DC system. IEEE Transactions on Applied Superconductivity, 26(4), 1-4.

[9] Yang, J. D., & Zhao, X. T. (2024). Study on Optimization of Low-Voltage Multi-Port Flexible Interconnection Device in AC/DC Hybrid Distribution. Journal of Nanoelectronics and Optoelectronics, 19(3), 307-316.

[10] Zhu, Z., Liu, D., Liao, Q., Tang, F., Zhang, J. J., & Jiang, H. (2018). Optimal power scheduling for a medium voltage AC/DC hybrid distribution network. Sustainability, 10(2), 318.

[11] Shekhar, A., Ramírez-Elizondo, L., Feng, X., Kontos, E., & Bauer, P. (2017). Reconfigurable dc links for restructuring existing medium voltage ac distribution grids. Electric Power Components and Systems, 45(16), 1739-1746.

[12] Feng, K., Xin, S., Zhang, P., Yang, J., Fan, C., & Chen, C. (2025). Optimizing deployment model of flexible interconnection systems for new energy 6/10 kV medium-voltage grids. International Journal of Low-Carbon Technologies, 20, 25-35.

[13] Shang, J., Yang, J., Xin, S., Xu, Q., Guo, M., & Niu, H. (2025). Analysis on dynamic characteristics and control strategy of medium structure network converter in new energy medium voltage flexible interconnection project. International Journal of Low-Carbon Technologies, 20, 90-98.

[14] WANG, Z., HUANG, W., ZHAO, C., CHEN, G., JIN, Z., & WANG, S. (2020). Research on flexible medium voltage DC distribution network with distributed generation. Journal of Electric Power Science and Technology, 35(1), 102-108.

[15] Wang, X., Yang, W., & Liang, D. (2021). Multi-objective robust optimization of hybrid AC/DC distribution networks considering flexible interconnection devices. IEEE Access, 9, 166048-166057.
[16] Xiao, H., Pei, W., Deng, W., Ma, T., Zhang, S., & Kong, L. (2021). Enhancing risk control ability of distribution network for improved renewable energy integration through flexible DC interconnection. Applied Energy, 284, 116387.
[17] Qiao, L., Li, X., Huang, D., Guo, L., Xu, Y., Tan, Z., & Wang, C. (2019). Coordinated control for medium voltage DC distribution centers with flexibly interlinked multiple microgrids. Journal of Modern Power Systems and Clean Energy, 7(3), 599-611.
[18] Shahbazi, Hamidreza, and Farid Karbalaei. "Decentralized voltage control of power systems using multi-agent systems." Journal of Modern Power Systems and Clean Energy 8.2 (2020): 249-259.
[19] Lijun Duan,Binghua Shi,Qiankun Zuo,Ruiheng Li,Hao Tian,Chao Wang & Haiyang Wang. (2025). Utilizing neutral GRC modeling based on resistive network for detecting geo-electrical structures and analyzing its impact on HVDC power grids. Ain Shams Engineering Journal,16(5),103375-103375.
[20] Waqas Saeed,Zhongyu Liu,Rubin Yan,Yuejun Li,Hongsheng Xu,Ye Tian... & Wei Liu. (2024). Nanostructured compliant interconnections for advanced Micro-Electronic packaging. Materials & Design,244,113166-113166.
[21] Yang Wang,Thomas Geury & Omar Hegazy. (2025). A Single-Phase Modular Multilevel Converter Based on a Battery Energy Storage System for Residential UPS with Two-Level Active Balancing Control. Energies,18(7),1776-1776.
[22] Ramudu Ganji,Kasukurthi Rambabu,Indira Damarla & B. Veeranarayana. (2025). A modified middleware submodule based modular multilevel converter topology to reduce the ripple components in the submodule voltage. Electrical Engineering,(prepublish),1-11.
[23] Xiaoyang Liu,Minghao Hui,Lu Fan,Wenwu Yu & Jinde Cao. (2025). Adaptive fuzzy funnel control of nonlinear multi-agent systems via dual-channel event-triggered strategy. Information Sciences,712,122129-122129.
[24] H. Li H, Y.X. Zhang, Y , S.J. Guo, et al. A comprehensive study on texture evolution and recrystallisation behaviour of Fe-50Co alloy, Electrical Materials and Applications, 1 (1) e12010, 2024.
[25] H. Sun, Y.L. Shang, Y. Han, et al. Research on magnetic field characteristics of amorphous alloy and grain-oriented silicon steel hybrid magnetic circuit iron core, Electrical Materials and Applications, 1 (2) e12014, 2024.
[26] X.Y. Wang, R.F. Xue, G Ma. Error analysis and correction strategy for measuring oriented silicon steel by SST method, 1 (2) e70002, 2024.